Volume-Averaged Stress States for Idealized Granular Materials using Unbonded Discrete Spheres in LS-DYNA®

Michael T. Davidson[1], Jae H. Chung[*1], Hailong Teng[2], Zhidong Han[2], Vinh Le[1]

[1] Bridge Software Institute, University of Florida, P.O. Box 116580, Gainesville, FL, 32611, USA
[2] Livermore Software Technology Corporation, 7374 Las Positas Rd., Livermore, CA, 94551, USA

[*]Corresponding author: JCHUN@CE.UFL.EDU

1 Introduction

The discrete element method (DEM) permits study of the kinetics of microscopic particles through use of the kinematics of contact mechanics, and has been used by numerous researchers to investigate kinematically admissible deformation fields observed in laboratory tests of Representative Elementary Volumes (REV) of granular masses. In the current study, newly-implemented discrete element analysis features within LS-DYNA are used to simulate three-dimensional (3D) quasi-static stress states for idealized bodies of granules subjected to quasi-static loading conditions. Operating within a 3D Cartesian domain, volume-averages of summed dyadic products of contact forces and branch vectors (obtained from LS-DYNA simulation results) are used to investigate stresses that develop across various regions of uniform, unbonded discrete element sphere (UDES) assemblies, where the contact forces arise due to body forces that are prescribed at the centroid of each sphere. When feasible, averaged local force results (micromechanical stresses) obtained from LS-DYNA simulations are compared to corresponding manual calculations. As demonstration of the LS-DYNA DEM capabilities, and as a means of showcasing a recently implemented stress computation algorithm specific to the use of UDES, volume-averaged stress quantities are investigated at three scales: 1) On an individual sphere within a two-dimensional simple, pyramidal assembly; 2) On an REV associated with laboratory-scale triaxial compression testing; and, 3) On multiple REVs sampled from a megascopic assembly. The as-demonstrated discrete element analysis of the particulate equations of motion can be applied to modeling of in-situ granular soil conditions, where geostatic stress equilibrium conditions can be simulated in relation to micro-mechanical model parameters.

2 Overview of Discrete Element Method for Unbonded Spheres

Originally developed in 1979 [1], the DEM has more recently been implemented in LS-DYNA [2]. As shown in Fig. 1, UDES are modeled as an ensemble of several rheological components (e.g., springs, dashpots, force boundaries of capillarity). Importantly, robust contact algorithms (such as the penalty spring methodology of LS-DYNA) drive the resultant effect of all active rheological forces acting on the spherical surface boundaries. Consequently, dynamic force equilibrium is maintained at the centroid of the UDES over the full variety of interactions.
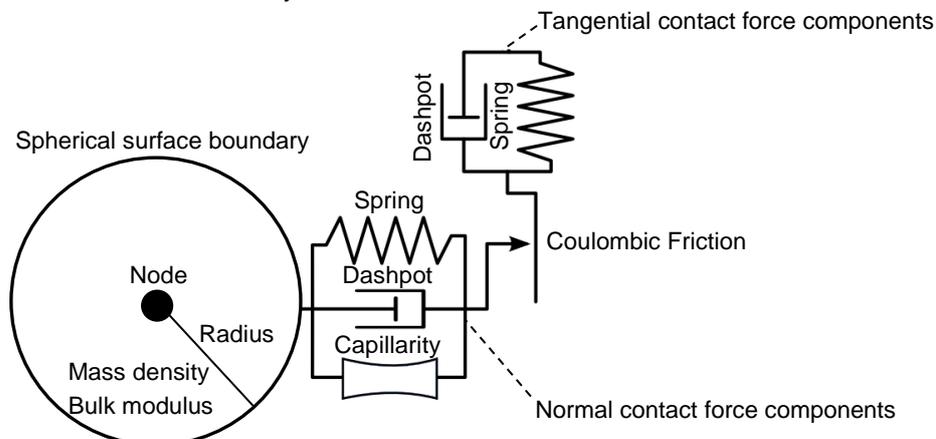

Fig.1:   Schematic of an unbonded discrete element sphere ([2]).

In the current study, the interactions among UDES are examined under steady states in which no transient flow occurs (i.e., quasi-static regimes). Therefore, the full complement of rheological components (Fig. 1) is not relevant to the current study. Accordingly, only selected rheological components are investigated herein: normal contact stiffness and Coulombic friction. Note that for all simulations conducted in the current study, the properties listed in Table 1 are utilized unless otherwise indicated.

Microscopic property	Value	Unit
Radius	2.5E-03	m
Density (by weight)	25.51	kN/m^3
Bulk modulus	3.33E+07	kPa
Spring stiffness (normal contact)	4.17E+04	kN/m
Coulombic friction coefficient	0.1 to 0.8	--

Table 1: UDES parameters.

2.1 Averaged Local Stresses over a Discrete Element Sphere

For a given, individual UDES in contact with other spheres, stresses that arise are a function of each vectorial contact force ($\vec{f}$) and the corrsponding vectorial distance ($\vec{b}$) from the sphere center to the point of contact. More specifically, the local stress tensor (σ^ℓ) is roughly approximated as a volume (V_{UDES}) average of the summed external work done by the contact forces for a given UDES, and for each of n contacts with adjacent spheres [3]:

$$\sigma_{ij}^\ell = \frac{1}{V_{UDES}} \sum_n \vec{f}_i \otimes \vec{b}_j \tag{1}$$

As demonstration of the UDES stress computation feature available in LS-DYNA, consider the top sphere of a three-sphere pyramid (Fig. 2). Note that the bottom row of spheres are restrained from motion, and all spheres are subjected to body forces through gravitational acceleration (9.81 m/s^2). By inspection, the two contact forces (F_1, F_2) acting on the lone top-row sphere are inclined at 60° and F_1, F_2 possess vertical components equal to one-half the body force (F_B). Given the magnitudes and orientations of the contact forces, and knowing the radius of the top-row sphere (Table 1), the corresponding volume-averaged stress components are calculated using Eqn. 1 and listed in Table 2. Comparisons of the manually calculated volume-averaged stress components to those computed using LS-DYNA for the top-row sphere show excellent agreement (Table 2).
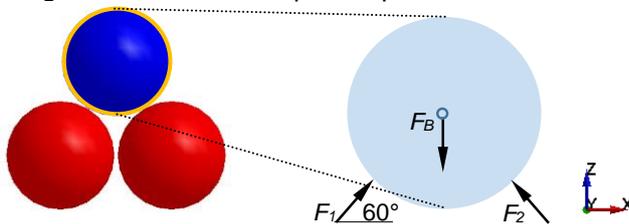

Fig.2: Pyramid of three unbonded UDES.

Local stress component	Manual calculation (kPa)	LS-DYNA (kPa)
σ_{xx}^ℓ	-1.84E-02 kPa	-1.85E-02 kPa
σ_{zz}^ℓ	-5.52E-02 kPa	-5.52E-02 kPa
$\sigma_{zx}^\ell = \sigma_{xz}^\ell$	0.00 kPa	0.00 kPa

Table 2: Comparisons of manually calculated and computed volume-averaged stresses.

3 Simulations of Triaxial Compression Testing

In contrast to the simple demonstration case discussed in Sec. 2 (recall Fig. 2, Table 2), the main objective of the current study is to simulate macroscopic stresses within bodies of megascopic, randomly packed assemblies of uniform UDES. As a means of progressing from simple assemblies (recall Fig. 2) to relatively more complex assemblies, while maintaining the feasibility of making manual estimates of volume-averaged stresses that can develop throughout said assemblies, triaxial compression tests [4] are carried out (Fig. 3).

3.1   Test Procedure

A 0.1 m diameter by 0.2 m long cylindrical triaxial compression test chamber (Fig. 3a) has been modelled using LS-DYNA. The numerical test procedure is divided into three stages: 1) Preparation of a specimen (i.e., collection of discrete element spheres); 2) Quasi-static application of an acceleration field and hydrostatic (confining) pressure; and, 3) Shearing of the specimen. Each stage of the triaxial compression test procedure, as modelled in LS-DYNA and detailed in Fig. 3, is discussed below.
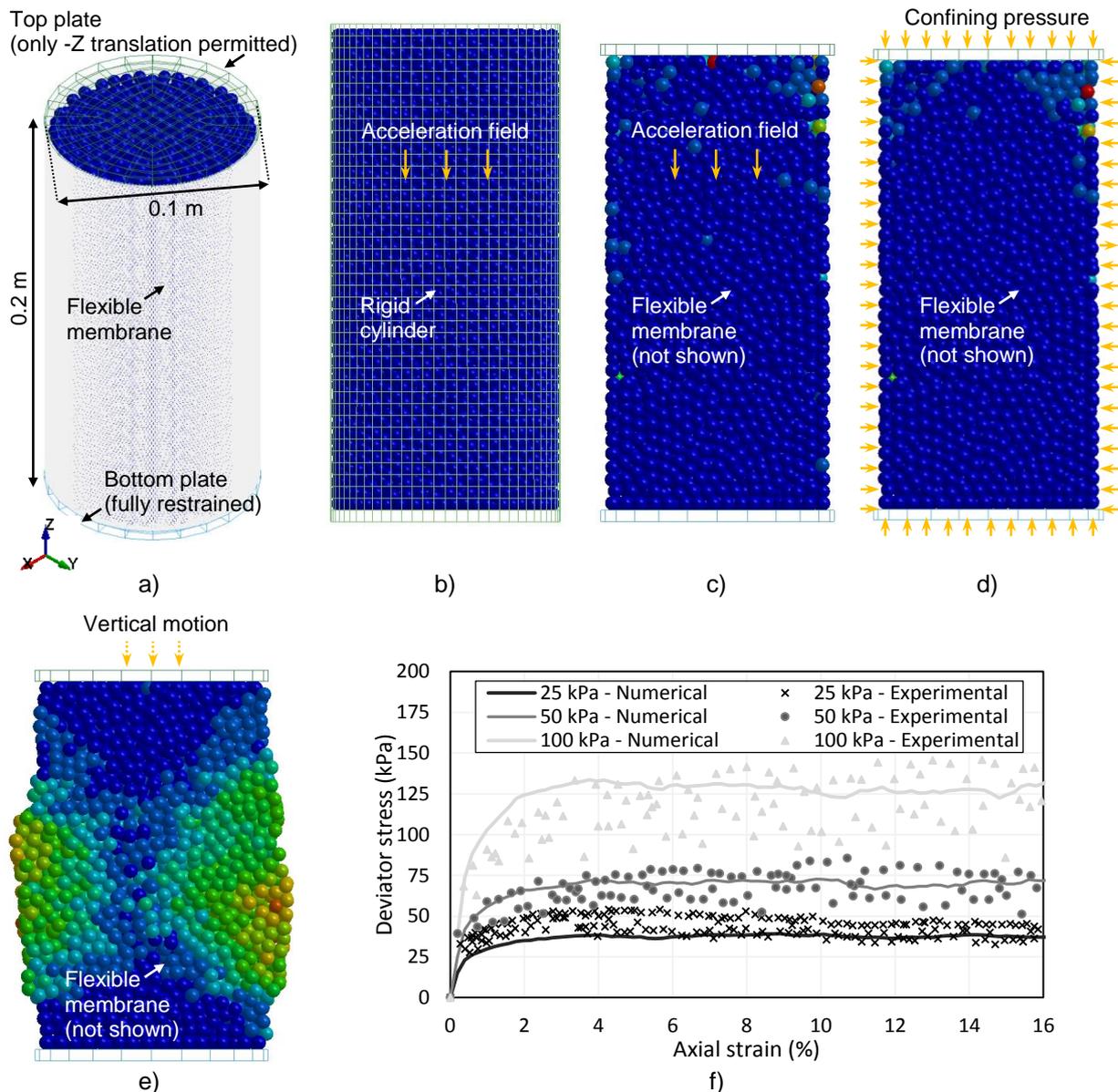

Fig.3:   Triaxial compression test model: a) Isometric view of packed sample; b) Sample packing; c) Sustained application of the acceleration field; d) Application of confining pressure; e) Depression of the top plate (displacement field shown); f) Validation against [6].

In the first stage of the triaxial compression test simulation, the LS-PREPOST algorithm for populating enclosed volumes with discrete element spheres [5] is iteratively employed to fill a rigid cylinder, which

in turn, is slightly longer than the 0.2 m triaxial compression test chamber (Fig. 3b). For each iteration of Stage 1, body forces are then quasi-statically imposed on each discrete element sphere of the specimen via gravitational acceleration (9.81 m/s^2) and by making use of the `*CONTROL_DYNAMIC_RELAXATION` feature [2]. The first stage of the overall procedure is concluded when the steady-state specimen positions correspond to a height of approximately 0.2 m, and by cataloguing the corresponding steady-state coordinates of each discrete element sphere. The second stage of the overall procedure is undertaken by initializing an identical set of discrete element spheres using the catalogued coordinates from Stage 1, but where (in Stage 2) the specimen is initialized inside the triaxial compression test apparatus (i.e., bounded by top and bottom plates and a flexible membrane). By again making use making use of the `*CONTROL_DYNAMIC_RELAXATION` feature [2], gravitational acceleration (Fig. 3c) and confining pressures (Fig. 3d) are quasi-statically imposed on the specimen. Subsequently, in Stage 3 of the procedure, and as afforded by the modelling of a flexible membrane (per [6]), shearing planes of arbitrary orientation can form as the top plate translates downward (Fig. 3e).

3.1.1 Validation of Triaxial Compression Test Model

The numerical triaxial compression test procedure and model (Fig. 3) is validated against physical measurements reported in [6], where plastic pearls were utilized in triaxial compression tests, and across a range of confining pressures (25 kPa, 50 kPa, and 100 kPa). Properties given in [6] for defining the numerical specimen (comprised of and corresponding to the plastic pearls) are listed in Table 3. As shown in Fig. 3f, triaxial compression test simulations that: 1) Follow the numerical testing procedure defined in Sec. 3.1; and, 2) Operate on specimens that are modelled using the properties listed in Table 3, lead to calculations of deviatoric shear stress versus axial strain that agree well with the corresponding (physical) experimental measurements.

Microscopic property	**Value**	**Unit**
Radius	3.25E-03	m
Density (by weight)	9.03	kN/m^3
Spring stiffness (normal contact)	2.00E+06	kN/m
Spring stiffness (tangential contact)	1.00E+06	kN/m
Coulombic friction coefficient	0.26	--

Table 3: Discrete element analysis parameters used in bench-marking of the triaxial compression test model.

3.2 Volume-Averaged Stresses over REV

In the current study, the 0.1 m diameter by 0.2 m long space (V_{REV}) occupied by the specimens is defined as an REV. If a macroscopic volume-averaged stress tensor is resolved into the summation of the dyadic products that develop for each sphere within V_{REV} [3], then:

$$\tilde{\sigma} = \frac{V_{REV} - V_{void}}{V_{REV}} \cdot \sum_m \left(\frac{1}{V_{UDES}} \sum_n \vec{f} \otimes \vec{b} \right) = (1-\eta) \cdot \sum_m \left(\frac{1}{V_{UDES}} \sum_n \vec{f} \otimes \vec{b} \right) \tag{2}$$

where V_{void} is the volume of voids and η is porosity. Relative to Eqn. 1, Eqn. 2 is additionally summed for each of m spheres, and the double summation is pre-multiplied by $(1-\eta)$. Inclusion of the pre-multiplier $(1-\eta)$ in Eqn. 2 constitutes a calculation of total stress based on the theory of mixtures.

The newly-implemented UDES stress computation feature in LS-DYNA is assessed within the context of the triaxial compression test simulations by investigating the volume-averaged stresses that develop with respect to the REV. More specifically, just prior to beginning Stage 3 of the numerical triaxial compression test procedure (recall Sec. 3.1), hydrostatic pressures are imposed on the specimens as a non-essential boundary condition. Therefore, just prior to beginning Stage 3 (in the simulations), the volume-averaged stress components should each be equal to the applied confining pressure (neglecting the specimen weight). As listed in Table 4, volume-averaged stresses across the

REV converge to the applied confining pressures for the three simulations making up the triaxial compression test validation.

Confining Pressure (kPa)	η	$\tilde{\sigma}_{XX}$ (kPa)	$\tilde{\sigma}_{YY}$ (kPa)	$\tilde{\sigma}_{ZZ}$ (kPa)
25	0.37	-25.0	-25.1	-26.0
50	0.37	-49.6	-49.8	-51.9
100	0.35	-98.1	-98.8	-106

Table 4: Applied confining pressures and corresponding volume-averaged stresses.

4 Simulations of Randomly Packed Assemblies Subjected to Body Forces

In contrast to the relatively straightforward means by which volume-averaged stresses are determined for individual spheres within a small assembly of spheres (recall Sec. 2.1), numerical models capable of capturing geostresses (at the macroscopic scale) that develop throughout large granular bodies may require the modelling of thousands or even millions of UDES, depending on the sizes of both REV and UDES. For the remainder of the current study, volume-averaged stresses that develop across selected subsets of spheres within multiple bodies of REVs are investigated. In addition, the effect of Coulombic friction (recall Table 1) is explored for otherwise identical simulations of quasi-static stress development in randomly packed assemblies.

4.1 Simulation Set

Using the microscopic properties listed in Table 1, including the eight values of Coulombic friction (from 0.1 to 0.8), eight corresponding rigid cylindrical containers are populated with approximately 1.26 million spheres (Fig. 4). Note that the algorithm implemented in LS-PREPOST [8] was again utilized in populating the cylindrical containers with uniform UDES. All spheres within the rigid cylindrical containers are subjected to body forces (via gravitational acceleration, 9.81 m/s^2) through use of the `*CONTROL_DYNAMIC_RELAXATION` feature [2] (Fig. 4b). Across the set of eight simulations, only the Coulombic friction coefficient is varied. Upon reaching convergence of the dynamic relaxation process, and thereby achieving mechanically stable states, stresses that develop throughout the uniform UDES assemblies are investigated.
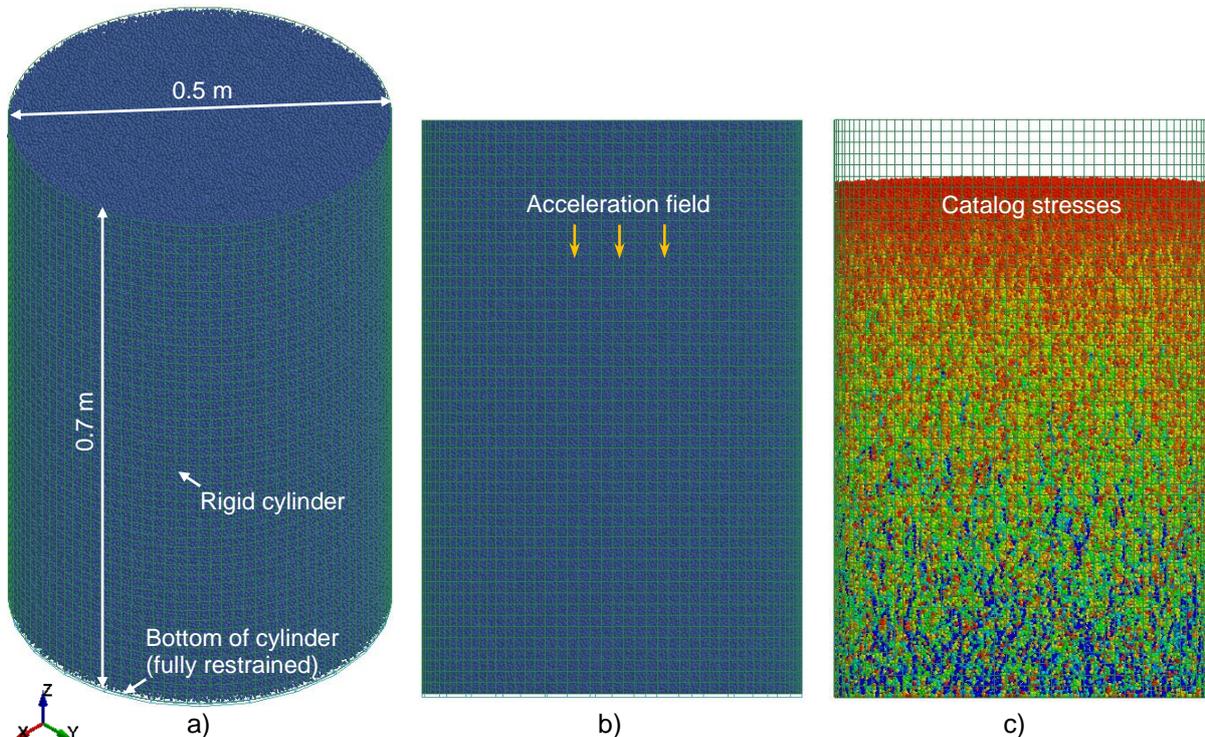

Fig.4: Simulation of uniform UDES subjected to body forces: a) Isometric view; b) Application of acceleration field; c) Cataloging of stresses.

4.2 Simulation Results

Volumetric properties of the full assemblies are listed for each of the eight simulations in Table 4: height (H_s), total volume (V_{total}), volume of solids (V_{solid}), volume of voids (V_{void}), and porosity (η). As expected, the full assembly height (H_s) and porosity (η) increase in proportion to increasing coefficients of Coulombic friction.

Friction coefficient	H_s (m)	V_{total} (m³)	V_{solid} (m³)	V_{void} (m³)	η
0.1	0.695	1.36E-01	8.24E-02	5.41E-02	0.396
0.2	0.706	1.39E-01	8.24E-02	5.61E-02	0.405
0.3	0.712	1.40E-01	8.24E-02	5.74E-02	0.411
0.4	0.713	1.40E-01	8.24E-02	5.76E-02	0.411
0.5	0.715	1.40E-01	8.24E-02	5.80E-02	0.413
0.6	0.715	1.40E-01	8.24E-02	5.80E-02	0.413
0.7	0.718	1.41E-01	8.24E-02	5.85E-02	0.415
0.8	0.723	1.42E-01	8.24E-02	5.96E-02	0.420

Table 5: Volumetric properties of the full assemblies over the range of microscopic sliding frictions considered.

4.2.1 Volume-Averaged Macroscopic Stresses

Three separate but consistent REVs (REV₁, REV₂, REV₃) are defined within the full assemblies, as shown in Figs. 5-6. Note that the dimensions of REV₁, REV₂, and REV₃ match that of the REV associated with the triaxial compression test model (recall Sec. 3). Specifically, for the eight simulations, each cylindrical REV is defined as 0.1 m in diameter and 0.2 m long. As a means of minimizing boundary effects (due to the presence of the rigid cylinder container), the REVs are sampled end-to-end along the vertical central axis of the rigid cylinder container (Fig. 6). Computed (volume-averaged) values of horizontal (X) and vertical (Z) stresses that develop across the REVs are listed in Tables 6-8.
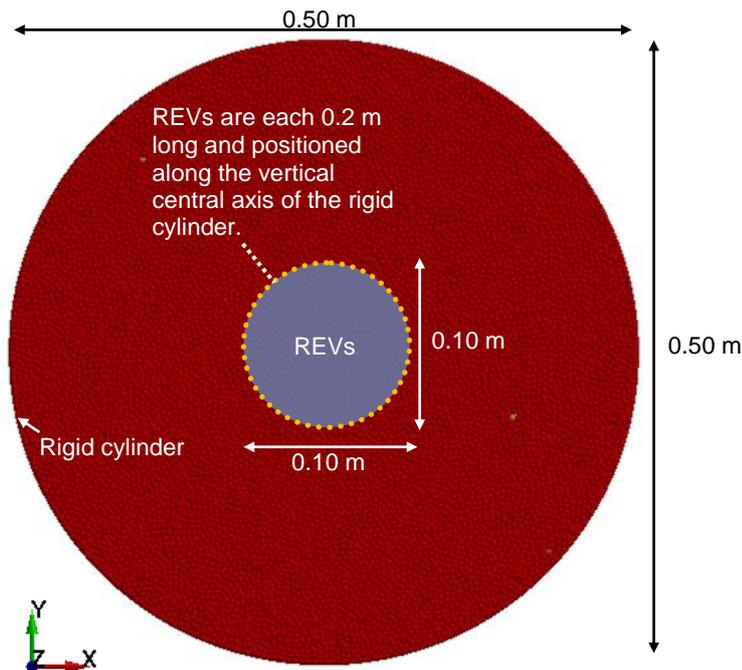

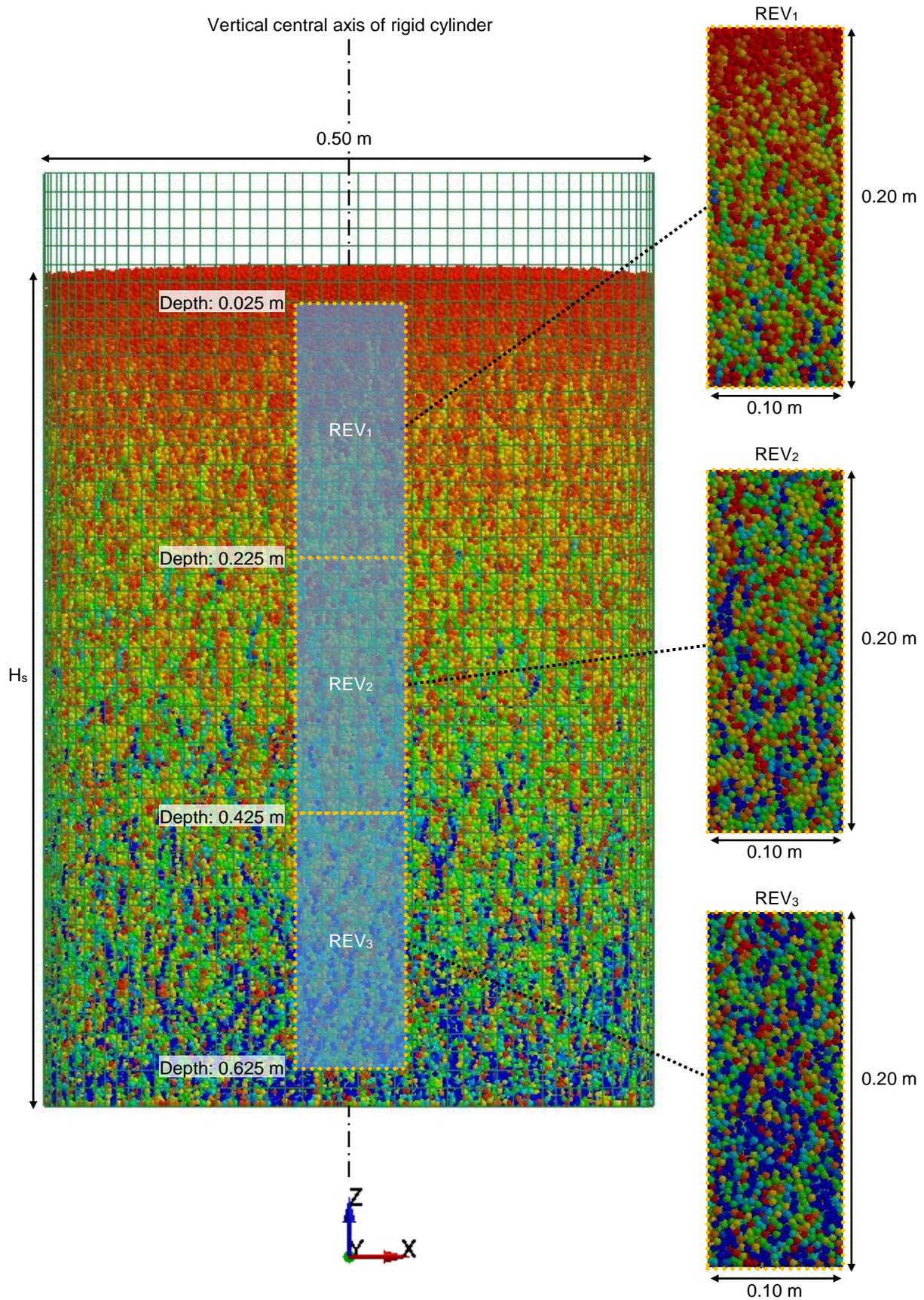*Fig.5: Locations of REVs in the randomly packed assemblies of uniform UDES (plan view).*

Fig.6: Positions of REVs in the randomly packed assemblies of uniform UDES (elevation view).

Friction coefficient	$\tilde{\sigma}_{xx}$ (kPa)	$\tilde{\sigma}_{zz}$ (kPa)	$\tilde{\sigma}_{xx}$ / $\tilde{\sigma}_{zz}$
0.1	-1.21	-1.42	0.85
0.2	-1.35	-1.63	0.83
0.3	-1.37	-1.7	0.81
0.4	-1.47	-1.87	0.79
0.5	-1.57	-2.14	0.73
0.6	-1.23	-1.98	0.62
0.7	-1.26	-2.01	0.63
0.8	-1.18	-2	0.59

Table 6: Volume-averaged stresses computed for REV₁

Friction coefficient	$\tilde{\sigma}_{xx}$ (kPa)	$\tilde{\sigma}_{zz}$ (kPa)	$\tilde{\sigma}_{xx}$ / $\tilde{\sigma}_{zz}$
0.1	-3.73	-4.17	0.89
0.2	-4.13	-4.70	0.88
0.3	-4.20	-4.98	0.84
0.4	-4.27	-5.16	0.83
0.5	-4.29	-5.22	0.82
0.6	-3.45	-4.47	0.77
0.7	-3.76	-4.87	0.77
0.8	-3.37	-4.60	0.73

Table 7: Volume-averaged stresses computed for REV₂

Friction coefficient	$\tilde{\sigma}_{xx}$ (kPa)	$\tilde{\sigma}_{zz}$ (kPa)	$\tilde{\sigma}_{xx}$ / $\tilde{\sigma}_{zz}$
0.1	-6.24	-7.56	0.83
0.2	-6.46	-7.68	0.84
0.3	-6.47	-8.05	0.80
0.4	-6.69	-8.34	0.80
0.5	-6.96	-8.61	0.81
0.6	-6.31	-7.98	0.79
0.7	-6.66	-8.41	0.79
0.8	-5.65	-7.18	0.79

Table 8: Volume-averaged stresses computed for REV₃

Comparative plots of $\tilde{\sigma}_{xx}$ for REV$_1$, REV$_2$, and REV$_3$ are presented in Fig. 7. Similarly, $\tilde{\sigma}_{zz}$ and ratios of $\tilde{\sigma}_{xx}$ to $\tilde{\sigma}_{zz}$ are presented in Fig. 8 and Fig. 9, respectively. As expected, the computed horizontal (Fig. 7) and vertical (Fig. 8) stress components indicate that the volume-averaged stresses become more compressive in proportion to increasing depth. Further, as expected, the ratios of $\tilde{\sigma}_{xx}$ to $\tilde{\sigma}_{zz}$ indicate consistent decreases in proportion to increasing levels of microscopic friction (Fig. 9).
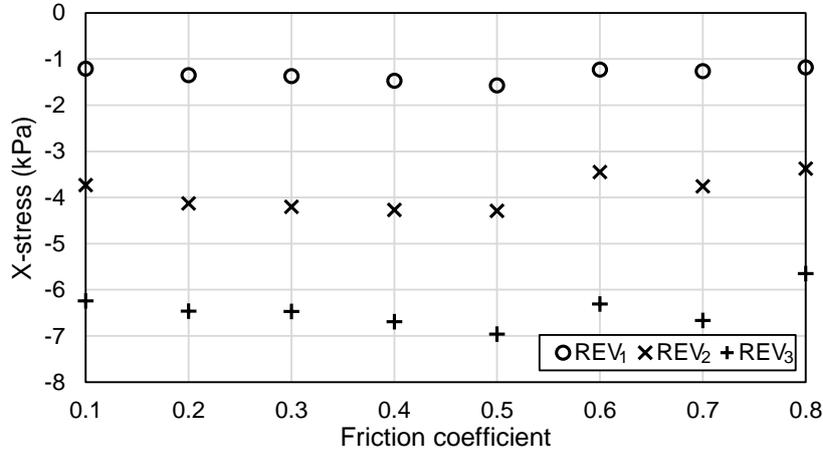

Fig.7: $\tilde{\sigma}_{xx}$ over the range of Coulombic friction coefficients considered
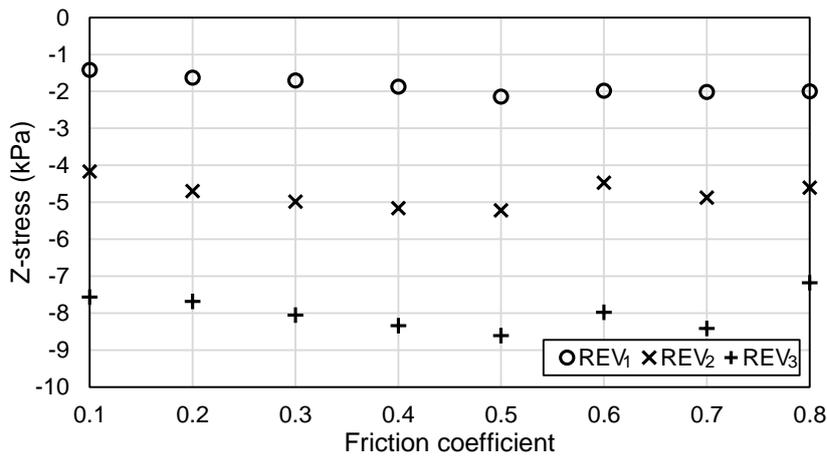

Fig.8: $\tilde{\sigma}_{zz}$ over the range of Coulombic friction coefficients considered
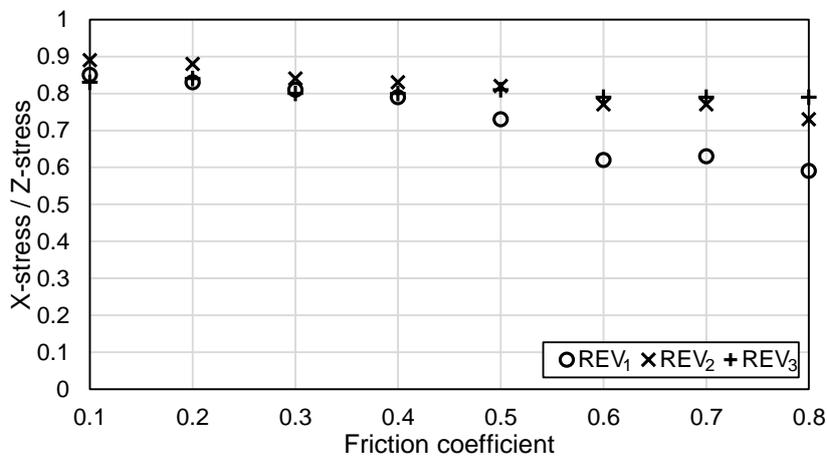

Fig.9: $\tilde{\sigma}_{xx} / \tilde{\sigma}_{zz}$ over the range of Coulombic friction coefficients considered

5 Summary

In this study, a newly-implemented stress calculation algorithm in LS-DYNA has been investigated, where volume-averaged stress calculations at both microscopic and macroscopic scales are made available for use in simulating assemblies of unbonded discrete element spheres. Volume-averaged stress calculations obtained from LS-DYNA simulation results were compared to manual estimates of corresponding stress quantities over a range of increasingly complex models. First, a case was considered wherein the local forces that develop on an individual sphere within a simple three-sphere assembly were calculated manually, and then, the manual calculations were shown to be in agreement with computed stresses obtained using LS-DYNA. Second, laboratory-scale models were validated against (physical) experimental measurements and then used to verify predictable quantities of volume-averaged stresses over a range of confining pressures. Third, various assemblies of more than 1 million uniform unbonded discrete element spheres were modelled to simulate the effect of body forces (induced via gravitational acceleration) and three-dimensional quasi-static stress states. Volume-averaged stresses that were catalogued across representative elementary volumes were then demonstrated to adhere to expected trends with respect to increasing depth and increasing levels of microscopic Coulombic friction. Summarily, discrete element stress computations implemented in LS-DYNA enable modelling of in-situ granular soil conditions. In turn, geostatic stress equilibrium conditions can be explicitly simulated per micro-mechanical properties (i.e., the numerical parameters hold physical meaning).

6 Literature

[1] Cundall, P. A., and Strack, O. D.: A discrete element model for granular assemblies. *Geotechnique* **29** (1979), 47-65.

[2] Livermore Software Technology Corporation (LSTC): *LS-DYNA Keyword User's Manual Vol. I*, (2015), Livermore, California, USA.

[3] Fortin, J., Millet, O., Saxcé de G.: Construction of an averaged stress tensor for a granular medium, *European Journal of Mechanics A/Solids*, **22** (2003), 567-582.

[4] ASTM: *Standard test method for consolidate drained triaxial compression test for soils D7181*, ASTM International, (2011), West Conshohocken, Pennsylvania, USA.

[5] Han, Z., Teng, H., and Wang, J.: Computer Generation of Sphere Packing for Discrete Element Analysis in LS-DYNA, (2012), *12th International LS-DYNA Conference*.

[6] Cil, M. B., and Alshibli, K. A.: 3D analysis of kinematic behavior of granular materials in triaxial testing using DEM with flexible membrane boundary. *Acta Geotechnica*, **9**(2). (2014), 287-298.